Masses for the Local Group and the Milky Way

Yang-Shyang Li[1]★ and Simon D. M. White[2]★

[1]*Kapteyn Astronomical Institute, PO Box 800, 9700 AV Groningen, the Netherlands*
[2]*Max-Planck-Institut für Astrophysik, Karl-Schwarzschild-Str. 1, D-85748 Garching, Germany*

ABSTRACT

We use the very large Millennium Simulation of the concordance Λ cold dark matter cosmogony to calibrate the bias and error distribution of Timing Argument estimators of the masses of the Local Group and of the Milky Way. From a large number of isolated spiral–spiral pairs similar to the Milky Way/Andromeda system, we find the interquartile range of the ratio of timing mass to true mass to be a factor of 1.8, while the 5 and 95 per cent points of the distribution of this ratio are separated by a factor of 5.7. Here, we define true mass as the sum of the 'virial' masses, M_{200}, of the two dominant galaxies. For present best values of the distance and approach velocity of Andromeda, this leads to a median likelihood estimate of the true mass of the Local Group of $5.27 \times 10^{12}\,\mathrm{M_{\odot}}$ or $\log M_{\mathrm{LG}}/\mathrm{M_{\odot}} = 12.72$, with an interquartile range of [12.58, 12.83] and a 5–95 per cent range of [12.26, 13.01]. Thus, a 95 per cent lower confidence limit on the true mass of the Local Group is $1.81 \times 10^{12}\,\mathrm{M_{\odot}}$. A timing estimate of the Milky Way's mass based on the large recession velocity observed for the distant satellite Leo I works equally well, although with larger systematic uncertainties. It gives an estimated virial mass for the Milky Way of $2.43 \times 10^{12}\,\mathrm{M_{\odot}}$ with a 95 per cent lower confidence limit of $0.80 \times 10^{12}\,\mathrm{M_{\odot}}$.

Key words: Galaxy: formation – galaxies: kinematics and dynamics – Local Group – dark matter.

1 INTRODUCTION

During the 1970s it became generally accepted that most, perhaps all, galaxies are surrounded by extended distributions of dark matter, so-called dark haloes (Einasto, Kaasik & Saar 1974; Ostriker, Peebles & Yahil 1974). These were soon understood to play an essential role in driving the formation and clustering of galaxies (White & Rees 1978). With the introduction of the cold dark matter (CDM) paradigm, these ideas took more concrete form, allowing quantitative predictions to be made both for the population properties (Blumenthal et al. 1984) and for the large-scale clustering (Davis et al. 1985) of galaxies.

Measurements of the fluctuation spectrum of the cosmic microwave background (Smoot et al. 1992; Spergel et al. 2003) and of the apparent acceleration of the cosmic expansion (Riess et al. 1998; Perlmutter et al. 1999) elevated the CDM model, in its variant with a cosmological constant (ΛCDM), to the status of a standard paradigm. At the same time, improving numerical techniques and faster computers have enabled detailed simulation of the formation and evolution of the galaxy population within this paradigm throughout a significant fraction of the observable Universe (Springel et al.

2005). Nevertheless, direct observational evidence for haloes as extended as the paradigm predicts around galaxies like our own has so far come only from statistical analyses of the dynamics of satellite galaxies (e.g. Zaritsky et al. 1997; Prada et al. 2003) and of the gravitational lensing of background galaxies (e.g. Seljak 2002; Mandelbaum et al. 2006) based on large samples of field spirals.

The earliest observational indication that the effective mass of the Milky Way (MW) must be much larger than its stellar mass came from the Timing Argument (TA) of Kahn & Woltjer (1959). These authors noted that the Local Group (LG) is dominated by the two big spirals, and that these are currently approaching each other at about $100\,\mathrm{km\,s^{-1}}$. (The next most-luminous galaxy is M33 which is probably about a factor of 10 less massive than M31 and the Galaxy.) This reversal of the overall cosmic expansion must have been generated by gravitational forces, and since the distance to the nearest external bright galaxy is much greater than that between M31 and the MW, these forces are presumably dominated by material associated with the two spirals themselves.

Kahn & Woltjer set up a simple model to analyse this situation – two point masses on a radial orbit. These were at pericentre (i.e. at zero-separation) at the big bang and must have passed through apocentre at least once in order to be approaching today. Clearly, this requires an apocentric separation larger than the present separation and an orbital period less than twice the present age of the Universe. Together these requirements put a lower limit on on the total mass

★E-mail: ysleigh@astro.rug.nl (Y-SL); swhite@MPA-Garching.MPG.DE (SDMW)

of the pair. A more precise estimate of the minimum possible mass is obtained from the parametric form of Kepler's laws for a zero angular momentum orbit:

$$r = a(1 - \cos \chi), \tag{1}$$

$$t = \left(\frac{a^3}{GM}\right)^{1/2} (\chi - \sin \chi), \tag{2}$$

$$\frac{\mathrm{d}r}{\mathrm{d}t} = \sqrt{\frac{GM}{a}} \frac{\sin \chi}{1 - \cos \chi}, \tag{3}$$

where r is the present separation, $\mathrm{d}r/\mathrm{d}t$ is the present relative velocity, a is the semimajor axis, χ is the eccentric anomaly, t is the time since the big bang (the age of the Universe) and M is total mass (Lynden-Bell 1981). Given observationally determined values for r, $\mathrm{d}r/\mathrm{d}t$ and t, these equations have an infinite set of discrete solutions for χ, a and M labelled by the number of apocentric passages since the big bang. The solution corresponding to a single apocentric passage gives the smallest (and only plausible) estimate for the mass, which is about $5 \times 10^{12} \, \mathrm{M}_\odot$ for present estimates of r, $\mathrm{d}r/\mathrm{d}t$ and t. Note that this is still a lower limit on the total mass, even within the simple point-mass binary model, since any non-radial motions in the system would increase its present kinetic energy and so increase the mass required to reverse the initial expansion and bring the pair to their observed separation by the present day (see Einasto & Lynden-Bell 1982).

As Kahn & Woltjer realized, this timing estimate of the total mass of the LG exceeds by more than an order of magnitude the mass within the visible regions of the galaxies, as estimated from their internal dynamics, in particular, from their rotation curves. Thus, 90 per cent of the mass must lie outside the visible galaxies and be associated with little or no detectable light. Modern structure formation theories like ΛCDM predict this mass to be in extended dark matter haloes with $M(r)$ increasing very roughly as r out to the point where the haloes of the two galaxies meet. Such structures have no well-defined edge, so any definition of their total mass is necessarily somewhat arbitrary. In addition, their dynamical evolution from the big bang until the present day is substantially more complex than that of a point-mass binary. Thus, the mass value returned by the TA cannot be interpreted without some calibration against consistent dynamical models with extended dark haloes.

A first calibration of this type was carried out by Kroeker & Carlberg (1991) using simulations of an Einstein–de Sitter CDM cosmogony. Here, we use the very much larger Millennium Simulation (Springel et al. 2005) to obtain a more refined calibration based on a large ensemble of galaxy pairs with observable properties similar to those of the LG. We find that the standard timing estimate is, in fact, an almost unbiased estimate of the sum of the conventionally defined virial masses of the two large galaxies.

Zaritsky et al. (1989) attempted to measure the halo mass of the MW alone by measuring radial velocities for its dwarf satellites and assuming the population to be in dynamical equilibrium in the halo potential. They noted, however, that one of the most-distant dwarfs, Leo I, has a very large recession velocity and as a result provides a interesting lower limit on the MW's mass by a variant of the original TA. To reach its present position and radial velocity, Leo I must have passed pericentre at least once since the big bang and now be receding from the Galaxy for (at least) the second time.

Applying the point-mass radial orbit equations (1)–(3) to this case gives a lower bound of about $1.6 \times 10^{12} \, \mathrm{M}_\odot$. This seems likely to be a significant underestimate, since Leo I could not have passed

through the centre of the MW without being tidally destroyed so its orbit cannot be purely radial. Below we calibrate the TA for this case also, finding it to work well although with significantly more scatter than for the LG as a whole. This is because the ΛCDM paradigm predicts that the dynamics on the scale of Leo I's orbit (∼200 kpc) is typically more complex than on the scale of the LG as a whole (∼700 kpc).

Our paper is organized as follows. In Section 2, we briefly describe the Millennium Simulation and the selection criteria we use to define various samples of 'LG-like' pairs and of 'MW-like' haloes. In Section 3, we plot the ratio of true total mass to TA mass estimate for these samples, and we use its distribution to define an unbiased TA estimator of true mass with its associated confidence ranges. In Section 3.2, this is then applied to the LG in order to obtain an estimate of its true mass with realistic uncertainties. Section 3.3 attempts to carry out a similar calibration for the TA-based estimate of the Galaxy's halo mass from the orbit of Leo I. We conclude in Section 4 with a summary and brief discussion of our results.

2 THE MILLENNIUM SIMULATION

The *Millennium Simulation* is an extremely large cosmological simulation carried out by the Virgo Consortium (Springel et al. 2005). It followed the motion of $N = 2160^3$ dark matter particles of mass $8.6 \times 10^8 \, h^{-1} \, \mathrm{M}_\odot$ within a cubic box of comoving size $500 \, h^{-1}$ Mpc. Its comoving spatial resolution (set by the gravitational softening) is $5 \, h^{-1}$ kpc. The simulation adopted the concordance ΛCDM model with parameters $\Omega_\mathrm{m} = 0.25$, $\Omega_\mathrm{b} = 0.045$, $h = 0.73$, $\Omega_\Lambda = 0.75$, $n = 1$ and $\sigma_8 = 0.9$, where, as usual, we define the Hubble constant by $H_0 = 100h \, \mathrm{km \, s^{-1} \, Mpc^{-1}}$. The present age of the Universe is then 13.6×10^9 yr. The positions and velocities of all particles were stored at 63 epochs spaced approximately logarithmically in expansion factor at early times and at approximately 300 Myr intervals after $z = 2$. For each such snapshot, a friends-of-friends (FOF) group-finder was used to locate all virialized structures, and their self-bound substructures (subhaloes) were identified using SUBFIND (Springel et al. 2001). Haloes and subhaloes in neighbouring outputs were then linked in order to build formation history trees for all the subhaloes present at each time. These data are publicly available at the Millennium release site.[1] A 'MW' halo at $z = 0$ typically contains a few thousand particles and several resolved subhaloes.

Galaxy formation was simulated within these merging history trees by using semi-analytic models to follow the evolution of the baryonic components associated with each halo/subhalo. Processes included are radiative cooling of diffuse gas, star formation, the growth of supermassive black holes, feedback of energy and heavy elements from supernovae and active galactic nuclei, stellar population evolution, galaxy merging and effects due to a re-ionizing ultraviolet background. The $z = 0$ galaxy catalogue we analyse here corresponds to the specific model of Croton et al. (2006) and details of its assumptions and parameters can be found in that paper. Data for the galaxy population at all redshifts are available at the Millennium web site for the updated model of De Lucia & Blaizot (2007), as well as for the independent galaxy formation model of Bower et al. (2006). All these models are tuned to fit a wide variety of data on the nearby galaxy population, and in addition fit many (but not all!) available data at higher redshift (see e.g. Kitzbichler & White 2006). The details of the galaxy formation modelling are not,

---

[1] http://www.mpa-garching.mpg.de/millennium

however, important for the dynamical issues which are the focus of our own paper.

At $z = 0$, there are 18.2×10^6 haloes/subhaloes identified in the simulation to its resolution limit of 20 particles. The galaxy formation model populates these with 8394 180 galaxies brighter than an absolute magnitude limit of $M_B = -16.7$ above which the catalogue can be considered reasonably complete. These catalogues list a number of properties for the haloes, subhaloes and galaxies which will be important for us. Galaxies are categorized into three types according to the nature of their association with the dark matter. A Type 0 galaxy sits at the centre of the dominant or main subhalo and can be considered the central galaxy of the halo itself (formally, of the FOF group). A Type 1 galaxy sits at the centre of one of the smaller non-dominant subhaloes associated with an FOF group. Finally, a Type 2 galaxy is associated to a specific particle and no longer has an associated subhalo because the object within which it formed was tidally disrupted after accretion on to a larger halo. Such galaxies merge with the central galaxy of their new halo after waiting for a dynamical friction time.

Each galaxy in the catalogue has an associated 'rotation velocity' V_{max}. This is the maximum of the circular velocity $V_c(r) = [GM(r)/r]^{1/2}$ of its subhalo for Types 0 and 1; for Type 2 objects V_{max} is frozen to its value at the latest time when the galaxy still occupied a subhalo. Type 0 and 1 galaxies also have an associated mass M_{halo} which is the mass of the self-bound subhalo which surrounds them. Finally, haloes of Type 0 galaxies have a conventional 'virial mass' M_{200}, defined as the total mass within the largest sphere surrounding them with an enclosed mean density exceeding 200 times the critical value. Below, we will consider both M_{halo} and M_{200} as possible definitions for the 'true' masses of M31 and the Galaxy.

We use the Millennium Simulation to construct samples of mock MW/Andromeda galaxies and of mock LGs as follows. We begin by identifying all Type 0 or Type 1 galaxies with characteristic 'rotation velocity' either in the narrow range $200 \leqslant V_{max} < 250 \, \text{km s}^{-1}$ or in the wider range, $150 \leqslant V_{max} < 300 \, \text{km s}^{-1}$. This produces samples of 166 090 and 699 177 galaxies, respectively. The exclusion of Type 2 galaxies reduces the samples by about 5–6 per cent in each case, but the excluded galaxies are in any case not plausible analogues for the LG giants since they are almost all members of large groups or clusters. We also consider subsamples in which the morphologies predicted by the semi-analytic model are forced to approximate those of M31 and the Galaxy. Specifically, we require a bulge-to-total luminosity ratio in the range $1.2 \leqslant M_{B, \text{bulge}} - M_{B, \text{total}} < 2.5$ so that the discs are two to nine times brighter than the bulges in the B band. This morphology cut reduces the samples in the two V_{max} ranges to 62 605 and 271 857 galaxies, respectively.

We then identify LG analogues in each of these four samples by identifying isolated pairs with separations in the range of 500–1000 kpc and with negative relative radial velocities. (Note that this is the true relative velocity rather than the relative peculiar velocity, that is, we have added the Hubble expansion to the relative peculiar velocity and have required the result to be negative.) We identify isolated pairs by keeping only those which have no 'massive' companion, defined as a galaxy with $V_{max} \geqslant 150 \, \text{km s}^{-1}$, within a sphere of 1 Mpc radius centred on the mid-point of the binary, and no nearby cluster, defined as a halo with $M_{200} > 3 \times 10^{13} \, \text{M}_\odot$ within 3 Mpc of the mid-point of the binary. These cuts ensure that the dynamics are dominated by mass associated with the two main systems, as appears to be the case for the LG. For galaxies selected in the narrower V_{max} range, we then find 178 pairs when the morphology cut is applied and 1128 pairs when it is not. For the wider V_{max}

range, the corresponding numbers are 2815 pairs and 16 479 pairs, respectively.

When calibrating the TA estimator, it proves advantageous to use simulated pairs with dynamical state quite close to that of the real LG. As we will see below, this eliminates some systems where the dominant motion is not in the radial direction and the TA therefore significantly underestimates the mass. We therefore make one final cut which requires the approach velocity of the two galaxies to lie between 0.5 and 1.5 times the value measured for the real system ($-130 \, \text{km s}^{-1}$). This results in our final sets of LG look-alikes. For the narrower V_{max} range, we end up with 117 pairs when the morphology cut is applied and 758 pairs when it is not, while for the wider V_{max} range the corresponding numbers are 1273 pairs and 8449 pairs, respectively.

When we study the application of the TA to the MW–Leo I system, we consider individual galaxies from both our V_{max} ranges. We require these to be isolated by insisting on that there should be no bright/massive companion (with luminosity exceeding 10 per cent of that of the host or $V_{max} > 150 \, \text{km s}^{-1}$) closer than 700 kpc and no massive group (defined as above) closer than 3 Mpc. This produces samples of 137 926 and 266 229 potential hosts in the cases with and without the morphology cut for the wider V_{max} range, and 29 245 and 57 816 potential hosts for the narrower range. We then search for Leo I analogues around these hosts by identifying companions in the separation range 200–300 kpc with $V_{max}(\text{comp}) \leqslant 80 \, \text{km s}^{-1}$, $M_B < -16.7$ and $V_{ra} \geqslant 0.7 V_{max}(\text{host})$, where V_{ra} is the relative radial velocity of the two objects and the last condition reflects the fact that Leo I is useful for estimating the MW's mass only because its recession velocity is comparable to the Galactic rotation velocity [$V_{ra} \sim 0.8 \, V_{max}(\text{host})$ for the real Leo I–MW system]. Pairs sharing the same MW-like host are excluded from the final list.

With these cuts, we find 344 and 896 satellite–host pairs in the samples with and without the morphology cut for the looser V_{max} range, and 168 and 374 for the tighter range. These relatively small numbers reflect the fact that only about 10 per cent of potential hosts actually have a faint companion in this distance range which is still bright enough to be resolved, and fewer than 5 per cent of these satellites are predicted to have positive recession velocities comparable to that observed.

3 RESULTS

3.1 Calibration of the Timing Argument mass for the Local Group

For each simulated LG analogue, the separation and relative radial velocity of the two galaxies can be combined with the age of the Universe (taken to be 13.6 Gyr) to obtain a TA mass estimate M_{TA}, equations (1)–(3). The true mass of the pair M_{tr} is harder to define because of the extended and complex mass distributions predicted by the ΛCDM model. The mass of an individual dark halo is often taken to be M_{200} the mass within a sphere of mean density 200 times the critical value, so a natural choice for M_{tr} is the sum of M_{200} for the two galaxies. The Millennium Simulation data base only lists M_{200} for Type 0 galaxies, those at the centre of the main subhalo of each FOF particle group. Many of our LG analogues lie within a single FOF group. One of the pair is then a Type 1 galaxy, the central object of a subdominant subhalo, and so has no listed value for M_{200}. In such cases, we have gone back to the particle data for the simulation in order to measure M_{200} directly also for these galaxies.

An alternative convention is to define M_{tr} as the sum of the values of M_{halo}, the maximal self-bound mass of each subhalo; this is
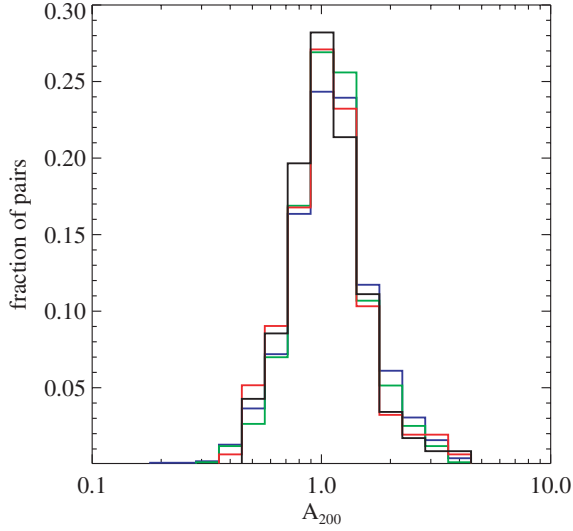
Figure 1. Normalized histograms of A_{200}, the ratio of true mass to TA estimate, for samples of LG analogues with $200 \leqslant V_{max} < 250\,km\,s^{-1}$ and $-195 < V_{ra} < -65\,km\,s^{-1}$. The black histogram refers to our preferred selection where both isolation and morphology requirements are imposed. For the red histogram, the isolation requirement has been removed, for the green histogram the morphology requirement has been removed, and for the blue histogram both requirements are relaxed.
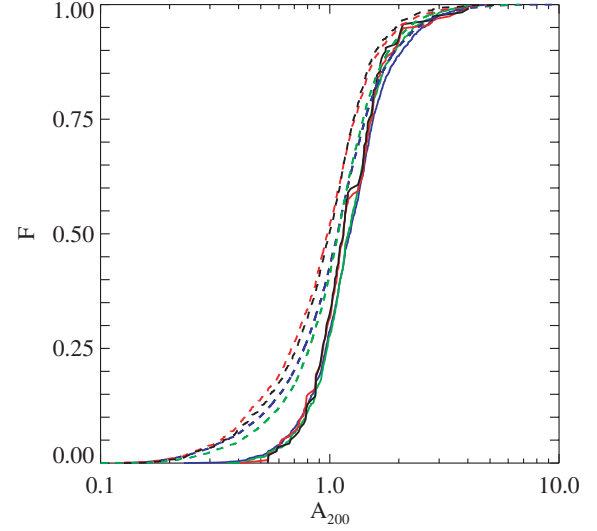

Figure 2. Cumulative distributions of A_{200}, the ratio of true mass to TA estimate, for LG analogues with $-195 < V_{ra} < -65\,km\,s^{-1}$. The solid curves correspond to the four samples already plotted in Fig. 1, while the dashed curves are for samples with $150 \leqslant V_{max} < 300\,km\,s^{-1}$. The colour coding is the same as in Fig. 1; black indicates samples with our preferred isolation and morphology constraints.

included in the data base for both Type 0 and Type 1 galaxies. In the following, we use the notation $M_{tr,200}$ and $M_{tr,\,halo}$ to distinguish between these two definitions. For either, we can calculate the ratio of true mass to TA estimate,

$$A_x = \frac{M_{tr,x}}{M_{TA}}, \tag{4}$$

where the suffix x is 200 or halo depending on the definition adopted for M_{tr}. If the TA is a good estimator of true mass, our samples of LG analogues should produce a narrow distribution of A values. This distribution then allows the TA mass estimate for the real LG to be converted into a best estimate of its true mass, together with associated confidence intervals.

Our preferred sets of LG analogues contain simulated galaxy pairs which mimic the real system in terms of morphology, isolation, pair separation and pair approach velocity. In addition, they require the haloes of the simulated galaxies to have V_{max} values within about ±10 and ±35 per cent of those estimated for M31 and the Galaxy for the tight and loose ranges of V_{max}, respectively. In order to understand the influence of these constraints, we give results below not only for our 'best' samples but also for samples where the various constraints are relaxed. Thus, we consider samples in which (i) both morphology and isolation requirements are applied (our preferred case), (ii) the isolation requirement is removed, (iii) the morphology requirement is removed, and (iv) both morphology and isolation requirements are removed. For each case, we compare results for the two allowed ranges of V_{max} and we also examine the effect of loosening the radial velocity constraint to $V_{ra} < 0$.

Fig. 1 gives histograms of the distribution of A_{200} for a sample in the narrow V_{max}-range with our preferred isolation, morphology and radial velocity cuts, as well as for three samples with the same V_{max} and V_{ra} cuts but with reduced morphology and isolation requirements. Fig. 2 presents these same distributions in cumulative form and compares them with the corresponding distributions for samples with the loosened circular velocity requirement, $150 \leqslant V_{max} <$

$300\,km\,s^{-1}$. In both plots, the black curves refer to class 1 samples for which both isolation and morphology cuts are imposed, while the red, green and blue curves refer to samples in classes 2, 3 and 4, respectively. Results for the broader V_{max} selection are indicated by the dashed curves in Fig. 2. We give numerical results for various percentile points of these distributions in Table 1, and repeat all these in Table 2 for samples where the separation velocity requirement has been loosened to $V_{ra} < 0$.

The first and most important point to note from these figures and tables is that the median value of A_{200} is very robust and only varies between 0.98 and 1.34 for our full range of sample selection criteria. With our preferred cuts, the median values are 1.15 and 0.99 for the narrow and wide V_{max} samples, respectively. The best estimate of the true mass of the LG (for this definition) is thus very similar to its TA mass estimate, and depends very little on the calibrating sample of simulated pairs.

The second important point is that the width of the distribution of A_{200} does depend on how the calibrating sample is defined. In particular, it is narrower for samples with the more restrictive V_{max} range, and for a given V_{max} range it is smallest for samples with our preferred cuts, those which match the dynamical and morphological properties of the LG most closely. For the narrow V_{max} sample, the interquartile range is a factor of just 1.6, and the upper and lower 5 per cent points are separated by a factor of 3. For the wider velocity range, the interquartile range is a factor of 1.8 and the 5 per cent points are separated by a factor of 5.7. This shows the TA to be remarkably precise for systems similar to the LG.

The broadening of the distribution as the selection requirements are relaxed is easy to understand. Removing the isolation requirements allows third bodies to play a significant role in the dynamics. This can extend the upper tail of the A_{200} distribution if mass from the third body falls inside R_{200} for one of the pair galaxies or if the gravity of the third galaxy produces a tidal field which opposes the attraction between the pair members. It can extend

Table 1. Percentage points of the A_{200} distribution for samples of LG analogues with $-195 < V_{ra} < -65 \, \text{km s}^{-1}$.

	5 per cent	25 per cent	50 per cent	75 per cent	95 per cent	Number of pairs
			$200 \leqslant V_{max} < 250 \, \text{km s}^{-1}$			
Morphology, isolation	0.67	0.93	1.15	1.47	2.05	117
Morphology, no isolation	0.61	0.93	1.14	1.52	2.09	155
No morphology, isolation	0.67	0.97	1.20	1.50	2.32	758
No morphology, no isolation	0.63	0.96	1.22	1.55	2.54	1015
			$150 \leqslant V_{max} < 300 \, \text{km s}^{-1}$			
Morphology, isolation	0.34	0.72	0.99	1.27	1.93	1273
Morphology, no isolation	0.33	0.68	0.98	1.29	2.00	1650
No morphology, isolation	0.41	0.81	1.09	1.40	2.21	8449
No morphology, no isolation	0.35	0.77	1.08	1.43	2.41	11838

Table 2. Percentage points of the A_{200} distribution for samples of LG analogues with $V_{ra} < 0$.

	5 per cent	25 per cent	50 per cent	75 per cent	95 per cent	Number of pairs
			$200 \leqslant V_{max} < 250 \, \text{km s}^{-1}$			
Morphology, isolation	0.54	0.97	1.33	1.66	3.93	178
Morphology, no isolation	0.45	0.94	1.26	1.66	3.93	241
No morphology, isolation	0.54	1.01	1.34	1.82	4.62	1128
No morphology, no isolation	0.42	0.96	1.34	1.93	5.11	1596
			$150 \leqslant V_{max} < 300 \, \text{km s}^{-1}$			
Morphology, isolation	0.28	0.85	1.19	1.64	3.30	2815
Morphology, no isolation	0.22	0.77	1.16	1.64	3.38	3532
No morphology, isolation	0.31	0.89	1.23	1.76	4.06	16479
No morphology, no isolation	0.18	0.79	1.19	1.78	4.46	23429

the lower tail if the mass of the third body lies between the pair members but outside their R_{200} spheres, thus enhancing their mutual attraction without adding to their mass. Removing the morphology constraint moves the whole distribution towards larger values and this effect is most pronounced in the large A_{200} tail. This is because objects with more dominant bulges have more complex merger histories. They typically form in denser regions and their haloes tend to be massive and to have more complex structure.

Loosening the requirements on V_{max} affects the distribution in a complex way. There is a tight relation between V_{max} and M_{200} (also M_{halo}) in the ΛCDM structure formation model (e.g. Navarro, Frenk & White 1997). Thus, if we place tight restrictions on the V_{max} values of our galaxies, we will obtain a sample of LG analogues with a narrow range of M_{tr} values. If, in addition, we force the parameters which enter in the TA (the pair separation and relative radial velocity) to lie in narrow ranges, then the TA mass estimate itself is tightly constrained. The distribution of A_{200} is thus forced to be narrow as a consequence of our selection criteria.

A second effect is that most of the new pairs added by widening the requirement on V_{max} have at least one galaxy with $150 \leqslant V_{max} < 200 \, \text{km s}^{-1}$, thus with relatively low M_{tr}. This simply reflects the strong dependence of halo abundance on V_{max}. Given that halo mass scales approximately as V_{max}^3, it is striking that the addition of so many pairs containing a 'low-mass' galaxy reduces the median value of A_{200} by just 15 per cent. The low tail of the distribution is more strongly affected, by almost a factor of 2 at the lower 5 per cent point, but the upper end of the distribution is barely affected at all. This demonstrates that the main body of the distribution is weakly affected by restrictions on V_{max}, but that the lower tail (which is needed to place a lower limit on the true

mass of the MW) is suppressed if V_{max} is not allowed to take small values.

In Table 2, we show the effect of weakening the cut on relative radial velocity to require only that the two main galaxies be approaching. Again this has remarkably little effect on the median A_{200} values. A comparison with Table 1 shows them all to be increased by about 10–15 per cent. The effects on the tails of the distributions are more substantial. The 95 per cent point is typically increased by about a factor of 2. This is because the sample now includes a substantial number of pairs with small V_{ra} (and thus smaller TA mass estimate) for which tangential motion is important for their present orbit. The 5 per cent point of the distribution is significantly reduced, reflecting the fact that our restrictions on relative approach velocity exclude a non-negligible number of systems with approach velocities *larger* than $195 \, \text{km s}^{-1}$, and thus with large TA mass estimates. Such systems must have more mass *outside* the conventional virial radii of the two galaxies than do typical LG analogues in our samples.

In conclusion, we believe our most precise and robust estimate of the distribution of A_{200} to be that obtained with our preferred morphology, isolation and radial velocity cuts for $150 \leqslant V_{max} < 300 \, \text{km s}^{-1}$, and we will use this distribution in the next section to estimate the true mass of the LG. Although the tails of the distribution are suppressed still further for a narrower range of V_{max}, this is at least in part due to the artificial effects mentioned above. In addition, the number of LG analogues is too small in this case for the tails of the distribution to be reliably determined. From Table 1, we see that the best estimate of the true mass of the LG (which we take to be that obtained using the median value of A_{200}) is almost identical to the direct TA estimate. The most-probable range of true mass (given by the quartiles of A_{200}) extends to values about 30 per cent

Table 3. Percentage points of the B_{200} distribution for samples of MW–Leo I analogues with $V_{\mathrm{ra}} \geqslant 0.7V_{\mathrm{max}}(\mathrm{host})$.

	5 per cent	25 per cent	50 per cent	75 per cent	95 per cent	Number of pairs
$200 \leqslant V_{\mathrm{max}}(\mathrm{host}) < 250\,\mathrm{km\,s}^{-1}$						
Morphology	0.71	1.27	1.71	2.01	2.62	168
No morphology	0.71	1.25	1.67	2.01	2.55	374
$150 \leqslant V_{\mathrm{max}}(\mathrm{host}) < 300\,\mathrm{km\,s}^{-1}$						
Morphology	0.39	1.04	1.50	1.89	2.47	344
No morphology	0.51	1.14	1.55	1.98	2.66	896

above and below this, while the 95 per cent confidence lower limit on the true mass (given by the 5 per cent point of the A_{200} distribution) is a factor of 2.9 smaller.

3.2 Application to the Local Group

The three observational parameters needed to make a TA mass estimate for the LG are the separation between the two main galaxies, their radial velocity of approach and the age of the Universe. The latter is now determined to high precision through measurements of microwave background fluctuations. Spergel et al. (2007) give 13.73 ± 0.16 Gyr. The distance to M31 is also known to high precision. We adopt the value 784 ± 21 kpc given by Stanek & Garnavich (1998) based on red clump stars, noting that it agrees almost exactly with the slightly less precise value obtained by Holland (1998) from fits to the colour–magnitude diagrams of M31 globular clusters. Although the heliocentric recession velocity of M31 is known even more precisely ($-301 \pm 1\,\mathrm{km\,s}^{-1}$ according to Courteau & van den Bergh 1999), the approach velocity of the two giant galaxies is less certain because of the relatively poorly known rotation velocity of the MW at the solar radius. van der Marel & Guhathakurta (2007) go through a careful analysis of the uncertainties and conclude that $V_{\mathrm{ra}} = 130 \pm 8\,\mathrm{km\,s}^{-1}$. Inserting these modern values into equations (1)–(3), we obtain our TA estimate of the mass of the LG:

$$M_{\mathrm{LG,TA}} \approx 5.32 \pm 0.48 \times 10^{12}\,\mathrm{M}_{\odot}, \tag{5}$$

where the uncertainty is dominated by that in the relative radial velocity. This uncertainty is still small in comparison to the scatter in the ratio of true mass to TA estimate, so we will neglect it in the following. The apocentric distance of the implied relative orbit of the two galaxies is 1103 ± 30 kpc.

We now combine this TA estimate with the distribution of A_{200} obtained in the last section for our most precise and reliable sample of LG analogues (the sample with our preferred morphology, isolation and radial velocity cuts and with the wider allowed range of V_{max}) to obtain our best estimate of the true mass of the LG, defined here as the sum of the M_{200} values of the two main galaxies:

$$M_{\mathrm{LG,\,true}} = 5.27 \times 10^{12}\,\mathrm{M}_{\odot}, \tag{6}$$

or $\log M_{\mathrm{LG,true}}/\mathrm{M}_{\odot} = 12.72$. The most-plausible range for this quantity is then [12.58, 12.83] with a 95 per cent confidence lower limit of 12.26, that is, $M_{\mathrm{LG,true}} > 1.81 \times 10^{12}\,\mathrm{M}_{\odot}$ at 95 per cent confidence.

3.3 Application to the Milky Way

We now calibrate the Zaritsky et al. (1989) TA which estimates the mass of the MW from the position and velocity of Leo I. This again assumes a radial Keplerian orbit, but Leo I is taken to have passed through pericentre and to be presently moving towards apogalacticon for the second time. Equations (1)–(3) then give a unique mass estimate $M_{\mathrm{MW,\,TA}}$ for the system for any assumed distance and radial
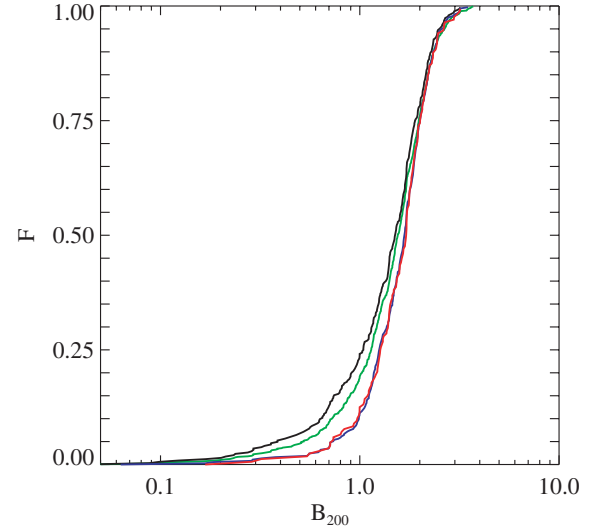
Figure 3. Cumulative distributions of B_{200}, the ratio of true MW mass (taken to be M_{200}) to TA estimate, for four samples of isolated MW–Leo I analogues from the Millennium Simulation. The red curve refers to MW analogues with $200 \leqslant V_{\mathrm{max}}(\mathrm{host}) < 250\,\mathrm{km\,s}^{-1}$ and with morphology matching the MW. For the black curve, the circular velocity requirement is loosened to $150 \leqslant V_{\mathrm{max}}(\mathrm{host}) < 300\,\mathrm{km\,s}^{-1}$, for the blue curve the morphology requirement is removed, and for the green curve both requirements are relaxed. In all cases, we require $V_{\mathrm{ra}} \geqslant 0.7V_{\mathrm{max}}(\mathrm{host})$.

velocity. This is taken as the MW's mass since the mass of Leo I is negligible in comparison.

Proceeding as for the LG, we select MW–Leo I analogues from the Millennium Simulation in order to study the relation of this TA estimate to the true mass of the MW, which we again take to be M_{200}. Thus, we define the ratio

$$B_{200} = \frac{M_{200}}{M_{\mathrm{MW,TA}}} \tag{7}$$

and investigate its distribution in various samples of analogue host–satellite systems. In particular, we consider samples of isolated host galaxies (as defined in Section 2) using both our looser and tighter V_{max} ranges, both with and without cuts on central galaxy morphology, and requiring the distance, radial velocity and maximum circular velocity of the satellite to satisfy $200 < r < 300$ kpc, $V_{\mathrm{ra}} \geqslant 0.7V_{\mathrm{max}}(\mathrm{host})$ and $V_{\mathrm{max}}(\mathrm{comp}) \leqslant 80\,\mathrm{km\,s}^{-1}$.

Results for these four samples are given in Table 3 and the corresponding cumulative distributions of B_{200} are plotted in Fig. 3. Scatter plots of M_{200} against $M_{\mathrm{MW,\,TA}}$ for the four samples are shown in Fig. 4. The behaviour is quite similar to that of the LG TA mass estimator A_{200}. The median value of B_{200} is robust and varies very little as the definition of the analogue sample is changed. Again it is 10–15 per cent smaller for samples with the looser V_{max} selection.
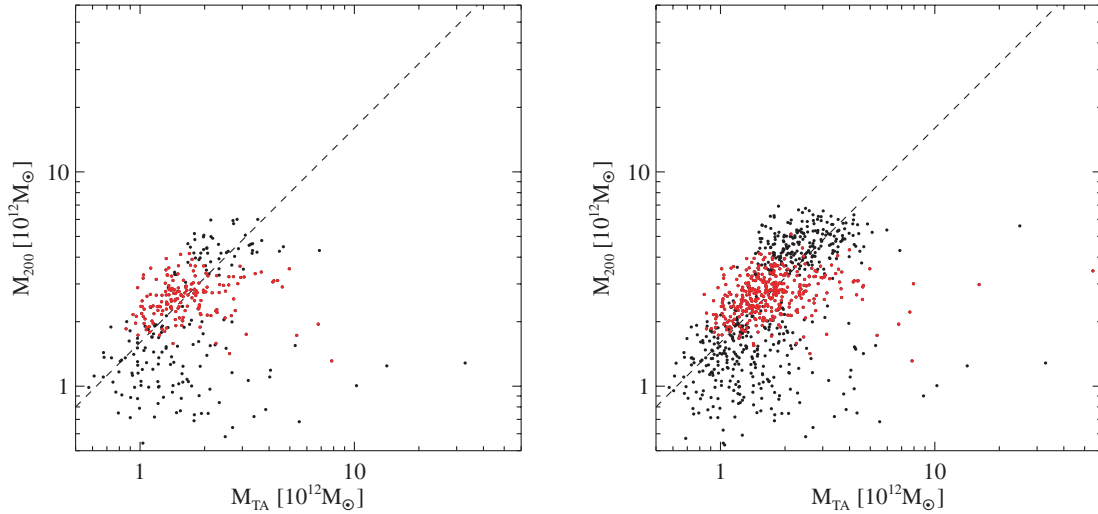
Figure 4. Scatter plots of the true mass, M_{200}, against its TA estimate of the 'MW's' mass. The left-hand panel is for isolated host galaxies with morphology matching that of the real MW, while the right-hand panel is for samples with no such morphology restriction. In both panels, the red dots refer to simulated host galaxies with $200 \leqslant V_{\max}(\text{host}) < 250 \,\text{km s}^{-1}$, while the black dots indicate other hosts in the broader range $150 \leqslant V_{\max}(\text{host}) < 300 \,\text{km s}^{-1}$. In all cases, the analogue of Leo I is required to have $200 < r < 300 \,\text{kpc}$, $V_{\text{ra}} \geqslant 0.7 V_{\max}(\text{host})$ and $V_{\max}(\text{comp}) \leqslant 80 \,\text{km s}^{-1}$. The straight dashed lines in the two panels show the approximate median relation $M_{200} = 1.6 \, M_{\text{MW,TA}}$

Unlike the LG case, the median value of B_{200} is about 1.6 and so is significantly larger than unity. This shows that $M_{\text{MW,TA}}$ is biased low as an estimator of true MW mass, reflecting the fact that tangential motions are often significant for satellites at the distance of Leo I. Assuming a purely radial orbit then results in an underestimate of the mass.

The width of the distribution of B_{200} is significantly greater for samples with the looser $V_{\max}$ selection, primarily through an extension of the tail towards low values. This resembles the behaviour we saw above for A_{200} but it must have a different cause, since our selection criteria for MW analogues put no upper bound on V_{ra}, instead placing a lower limit on $V_{\text{ra}}/V_{\max}$. As a result they do not force an upper limit on $M_{\text{MW,TA}}$ of the kind imposed on $M_{\text{LG,TA}}$ by our upper limit on V_{ra} for LG analogues. Fig. 4 shows that the tail of low B_{200} values for the wider $V_{\max}$ range is caused by a relatively small number of systems for which $M_{\text{MW,TA}}$ is anomalously large. These are objects with anomalously large values of V_{ra} and seem to occur preferentially at small M_{200}, corresponding to values of $V_{\max}$ below $200 \,\text{km s}^{-1}$.

The bulk of the points in Fig. 4 scatter fairly symmetrically about the median relation $M_{200} = 1.6 \, M_{\text{MW,TA}}$ which we show as a dashed straight line. Their mean slope is somewhat steeper than strict proportionality because our distance constraint on 'Leo I's' is expressed in units of kpc rather than R_{200} or $V_{\max}/H_0$. Distant outliers occur only at the low-M_{200} side of this relation, suggesting that they may be a consequence of resolution problems in the Millennium Simulation. For $V_{\max} \sim 150 \,\text{km s}^{-1}$, typical haloes are represented by fewer than 1000 particles and it seems likely that difficulties in describing the dynamics of their satellite substructures may begin to surface. In addition, the sample sizes are relatively small, particularly when we impose a morphology cut, so that the estimates of the tails of the distributions may be noisy. This may explain in part the apparent excess of outliers in the morphology-selected sample with the wider $V_{\max}$ range.

The observational data needed to obtain the TA estimate of the MW's mass are the age of the Universe and the Galactocentric distance and radial velocity of Leo I. As above, we take the age of

the Universe to be 13.73 ± 0.16 Gyr from Spergel et al. (2007). For the heliocentric distance to Leo I, we adopt $254 \pm 19 \,\text{kpc}$ from Bellazzini et al. (2004). The heliocentric radial velocity of Leo I is very precisely determined, $283 \pm 0.5 \,\text{km s}^{-1}$ according to Mateo, Olszewski & Walker (2007). Based on an assumed Galactic rotation speed at the Sun of $220 \pm 15 \,\text{km s}^{-1}$, we derive a corresponding Galactocentric radial velocity of $175 \pm 8 \,\text{km s}^{-1}$. When substituted into equations (1)–(3), these parameters produce a TA estimate for the MW's mass of

$$M_{\text{MW, TA}} = 1.57 \pm 0.20 \times 10^{12} \, M_{\odot}. \tag{8}$$

As was the case for the LG, the fundamental observational quantities are so well defined that the uncertainty of this estimate is much smaller than the expected scatter in B_{200}. We will therefore neglect it in the following. The implied apocentric distance of Leo I is $619 \pm 26 \,\text{kpc}$. Since this is about half the apocentric distance of the M31–MW relative orbit in the TA model of Section 3.2, perturbations of the orbit of Leo I due to the larger scale dynamics of the LG seem quite likely.

For the reasons discussed above, we consider our most-precise and robust estimate for the distribution of B_{200} to be that obtained for host galaxies with $150 \leqslant V_{\max}(\text{host}) < 300 \,\text{km s}^{-1}$ and with no morphology cut. The median of this distribution then gives our best estimate of the true halo mass of the MW:

$$M_{\text{MW, 200}} = 2.43 \times 10^{12} \, M_{\odot}, \tag{9}$$

or $\log M_{200}/M_{\odot} = 12.39$. The quartiles of the distribution imply [12.25, 12.49] for the most-probable range of this quantity, while the 5 per cent point implies a lower limit of 11.90 at 95 per cent confidence. Thus, the implied mass of the MW is roughly half that of the LG as a whole, as might be expected on the basis of the similarity of the two giant galaxies. It is quite similar to other recent estimates based on applying equilibrium dynamics to the system of distant MW satellites and halo stars (e.g. Wilkinson & Evans 1999; Sakamoto, Chiba & Beers 2003). A significantly smaller estimate came from the analysis of the high-velocity tail of the local stellar population by Smith et al. (2007), but we note that such analyses,
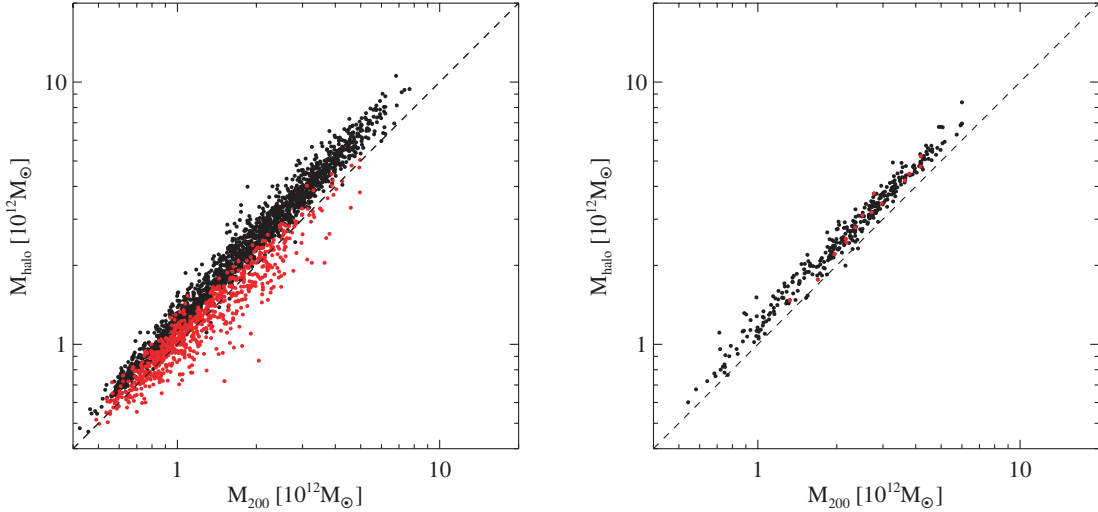
Figure 5. In the left-hand panel, we plot M_{halo} against M_{200} for all the galaxy (sub)haloes in our sample of LG analogues with our preferred morphology, isolation and radial velocity cuts and with $150 \leqslant V_{max} < 300 \, km \, s^{-1}$. Type 0 subhaloes are plotted black, while Type 1 subhaloes are plotted red. The diagonal line is the one-to-one relation. The right-hand panel is a similar plot for the 'MW' haloes in our preferred sample of MW–Leo I analogues.

in reality, only place a lower limit on the mass of the halo, since the distribution of solar neighbourhood stars may well be truncated at energies significantly below the escape energy.

3.4 An alternative mass measure?

The halo masses we have quoted so far have been based on the 'virial masses' M_{200} of simulated haloes. This choice is, of course, somewhat arbitrary, and it may not correspond particularly well to the radii within which individual isolated haloes are approximately in static equilibrium. As an alternative convention, we here consider defining the mass of an individual halo to be that of the corresponding self-bound subhalo identified by the SUBFIND algorithm of Springel et al. (2001). This algorithm typically includes material outside the radius R_{200} within which M_{200} is measured, but it excludes any material which is identified as part of a smaller subhalo orbiting within the larger system. In this paper, we denote this subhalo mass as M_{halo}.

In the left-hand panel of Fig. 5, we plot M_{halo} against M_{200} for all haloes in our preferred sample of LG analogues, that with our preferred morphology, isolation and radial velocity cuts and with $150 \leqslant V_{max} < 300 \, km \, s^{-1}$. The black and red points in this plot refer to Type 0 and Type 1 subhaloes, respectively. The right-hand panel of Fig. 5 is a similar plot for the 'MW' haloes in our preferred sample of MW–Leo I analogues, again the sample which is matched in morphology and which has the wider V_{max} range. In both panels, it is clear that the correspondence between the two mass definitions is quite tight, and that M_{halo} tends to be somewhat larger than M_{200}. In addition, the left-hand panel shows that Type 1 haloes have smaller M_{halo} for given M_{200} than do Type 0 haloes, as would naively be expected. The average value of $\log M_{halo}/M_{200}$ for the haloes in the left-hand panel is 0.100 for the Type 0 haloes and -0.004 for the Type 1 haloes, while it is 0.079 for the 'MW' haloes in the right-hand panel.

This close correspondence between the two mass definitions carries over to the distribution of our ratios of 'true' mass to timing mass. In Table 4, we give percentage points of the A_{halo} distribution for the eight samples of LG analogues already considered above. They can be compared directly with the numbers given in Table 1

for these samples. To a good approximation, the distribution of A_{halo} agrees with that of A_{200} except that all values are shifted upwards by about 16–20 per cent.

The same is also true for estimates of the MW's mass obtained using the TA applied to Leo I. This can be seen from Table 5 which repeats Table 3 except that we now give percentage points for B_{halo} rather than B_{200}. Clearly, it is of rather little importance which definition of halo mass we adopt: the results obtained with our two definitions are very similar.

4 DISCUSSION AND CONCLUSIONS

The statistical argument underlying the analysis of this paper is more subtle than it may at first appear, so it is worth restating it somewhat more formally in order to understand what is being assumed in deriving the mass estimates for the LG and for the MW given above.

We believe that the mass distributions around galaxies are much more extended than the visible stellar distributions, and that these have been assembled from near-uniform 'initial' conditions in a manner at least qualitatively resembling that in a ΛCDM universe. Thus, the assembly histories of the LG and of the MW's halo differ in major ways from those assumed by the original TAs of Kahn & Woltjer (1959) and Zaritsky et al. (1989). In addition, the meaning of the derived mass values needs clarification. We wish to use the Millennium Simulation to calibrate the TA estimates against conventional measures of halo mass, and to test the general applicability of the TA. However, we want to do this in a way which avoids any significant dependence on the details of the ΛCDM model, for example, on the exact density profiles, abundances and substructure properties which it predicts for haloes.

Our method uses the simulation to estimate the distribution of the ratio of 'true' mass to TA mass estimate for samples of objects whose properties 'resemble' those of the observed LG and MW–Leo I systems. Our restrictions on separation and radial velocity implement this similarity requirement in a straightforward way, but our constraints on V_{max} have a more complex effect. Although the true V_{max} values for M31 and the MW are very likely within our looser range ($150 \leqslant V_{max} < 300 \, km \, s^{-1}$), the simulation exhibits a tight correlation between V_{max} and M_{200}. Imposing fixed limits

Table 4. Percentage points of the A_{halo} distribution for samples of LG analogues with $-195 < V_{ra} < -65\,\mathrm{km\,s^{-1}}$.

	5 per cent	25 per cent	50 per cent	75 per cent	95 per cent	Number of pairs
			$200 \leqslant V_{max} < 250\,\mathrm{km\,s^{-1}}$			
Morphology, isolation	0.78	1.11	1.36	1.72	2.38	117
Morphology, no isolation	0.69	1.14	1.36	1.77	2.39	155
No morphology, isolation	0.76	1.17	1.44	1.75	2.74	758
No morphology, no isolation	0.71	1.15	1.44	1.82	2.97	1015
			$150 \leqslant V_{max} < 300\,\mathrm{km\,s^{-1}}$			
Morphology, isolation	0.41	0.88	1.20	1.53	2.26	1273
Morphology, no isolation	0.38	0.84	1.19	1.54	2.38	1650
No morphology, isolation	0.49	0.99	1.31	1.67	2.60	8449
No morphology, no isolation	0.37	0.92	1.30	1.71	2.85	11 838

Table 5. Percentage points of the B_{halo} distribution for samples of MW–Leo I analogues with $V_{ra} \geqslant 0.7 V_{max}$ (host).

	5 per cent	25 per cent	50 per cent	75 per cent	95 per cent	Number of pairs
			$200 \leqslant V_{max}$ (host) $< 250\,\mathrm{km\,s^{-1}}$			
Morphology	0.90	1.53	1.98	2.40	3.14	168
No morphology	0.90	1.50	1.97	2.39	3.21	374
			$150 \leqslant V_{max}$ (host) $< 300\,\mathrm{km\,s^{-1}}$			
Morphology	0.42	1.25	1.81	2.31	3.09	344
No morphology	0.61	1.37	1.88	2.36	3.23	896

on V_{max} is thus effectively equivalent to choosing a fixed range of M_{200}. As a result, we are in practice estimating the distribution of A_{200} or B_{200} for systems of given *true* mass, subject to the assumed constraints on separation and radial velocity. However, when we apply our results to estimate true masses for the LG and the MW, we implicitly assume that our distributions of A_{200} and B_{200} are appropriate for samples of given TA mass estimate, again subject to our constraints on separation and radial velocity. It is thus important to understand when these two distributions can be considered the same.

The relation can be clarified as follows. From the simulation, we compile the distribution of M_{tr}/M_{TA}, or equivalently of $\Delta \equiv \ln M_{tr} - \ln M_{TA}$, for systems with $\ln M_{tr}$ in a given range. We then implicitly assume that this distribution does not depend on M_{tr}, at least over this range, so that the result can be taken as an estimate of the probability density of Δ at given M_{tr}. Bayes Theorem then gives us the probability density function (pdf) for Δ at fixed M_{TA}:

$$
\begin{aligned}
f[\Delta|\ln M_{TA}] &= \frac{f[\Delta, \ln M_{TA}]}{f[\ln M_{TA}]} \\
&= \frac{f[\Delta, \ln M_{tr}]}{f[\ln M_{TA}]} \\
&= \frac{f[\Delta|\ln M_{tr}]\, f[\ln M_{tr}]}{f[\ln M_{TA}]} \\
&= f[\Delta|\ln M_{tr}].
\end{aligned}
\tag{10}
$$

The first line here simply writes the conditional pdf of Δ at given M_{TA} in terms of the joint pdf of the two quantities and the pdf of M_{TA}. The second line then rewrites the joint pdf in terms of the equivalent variables Δ and M_{tr}, using the fact that the Jacobian of the transformation is unity. The third line re-expresses the joint pdf as the product of the pdf of Δ at given M_{tr} times the pdf of M_{tr}. The final line then follows from the normalization condition, *provided* that $f[\ln M_{tr}]$ is constant and $f[\Delta|\ln M_{tr}]$ is independent of M_{tr}. Thus, when estimating M_{tr} from M_{TA}, we assume a uniform prior on $\ln M_{tr}$ and that the distribution of Δ does not depend on true mass. Both these assumptions appear natural and appropriate.

The analysis underlying the TA equations (1)–(3) assumes that the relative orbit of the two objects is bound and has conserved energy since the big bang. Recently, Sales et al. (2007) have shown that in ΛCDM models this assumption is significantly violated for a substantial number of satellites within haloes comparable to that of the MW. In particular, they demonstrate the presence of a tail of unbound objects which are being ejected from haloes as a result of three-body 'slingshot' effects during their first pericentric passage. These objects are typically receding rapidly from their 'MW', as assumed in the Zaritsky et al. (1989) argument, but they violate its assumption that the present orbital energy can be used to infer the period of the initial orbit (i.e. the time from the big bang to first pericentric passage). Clearly, such objects should also be present in the Millennium Simulation, although lack of resolution might make them underrepresented in comparison to the simulations analysed by Sales et al. (2007). Thus, our analysis takes the possibility of such ejected satellites into account, at least in principle. Objects of this type will show up as systems with anomalously large TA estimates for their halo mass, and Fig. 4 shows a number of outliers which could well be explained in this way. Issues of this kind do not affect TA-based estimates of the mass of the LG since the two big galaxies are presently approaching for the first time.

The only kinematic information about the relative orbit of M31 and the MW used in our analysis is their present approach velocity. van der Marel & Guhathakurta (2007) show that geometric arguments can already constrain the transverse component also, and future astrometry missions such as *SIM* might allow V_{tr} to be measured directly. Thus, it is interesting to ask if our TA mass estimate could be significantly refined by measuring the full three-dimensional relative motion of the two galaxies, rather than just its radial component. We address this in Fig. 6 which plots A_{200}, the ratio of true mass to TA estimate, against V_{tr} for a sample of LG analogues with our preferred morphology, isolation and radial velocity cuts, and with $150 \leqslant V_{max} < 300\,\mathrm{km\,s^{-1}}$. The median V_{tr} for this sample is $86\,\mathrm{km\,s^{-1}}$, comparable to the van der Marel & Guhathakurta (2007) estimate for the real system. There is no apparent correlation of A_{200} with V_{tr} and, indeed, the medians of A_{200} for the high- and low-V_{tr}